International Journal of Heat and Fluid Flow 30 (2009) 1026–1035

Contents lists available at ScienceDirect

International Journal of Heat and Fluid Flow

journal homepage: www.elsevier.com/locate/ijhff

Effects of free-stream turbulence on a transitional separated–reattached flow over a flat plate with a sharp leading edge

Zhiyin Yang [a,*], Ibrahim E. Abdalla [b]

[a] Department of Aeronautical and Automotive Engineering, Loughborough University, Loughborough LE11 3TU, UK
[b] School of Engineering and Technology, De Montfort University, Leicester LE1 9BH, UK

ARTICLE INFO

Article history:
Received 30 July 2008
Received in revised form 8 April 2009
Accepted 27 April 2009
Available online 22 May 2009

Keywords:
Large-eddy simulation
Transitional separated–reattached flow
Free-stream turbulence
Low-frequency flapping

ABSTRACT

The transitional separated–reattached flow on a flat plate with a blunt leading edge under 2% free-stream turbulence (FST) is numerically simulated using the Large-eddy simulation (LES) approach. The Reynolds number based on the free-stream velocity and the plate thickness is 6500. A dynamic subgrid-scale model is employed and the LES results compare well with the available experimental data.

It is well known that FST enhances shear-layer entrainment rates, reduces the mean reattachment distance, and causes early transition to turbulence leading to an early breakdown of the separated boundary layer. Many experimental studies have shown that different vortex shedding frequencies exist, specially the so called low-frequency flapping when there is a separation bubble but its mechanism is still not completely understood. The previous study by us without free-stream turbulence (NFST) did not show the existence of such a low-frequency flapping of the shear layer and it is not clear what the effects of FST will have on these shedding modes. Detailed analysis of the LES data has been presented in the present paper and the low-frequency flapping has not been detected in the current study.

1. Introduction

Many studies on separated–reattached flows have been carried out in the past decades due to their practical engineering importance. One of the fundamental features of this type of flows is two different shedding modes. The characteristic frequency shedding mode is associated with the usual large scale motions in the free shear layer while the low-frequency mode reflects overall separation bubble growth/decay dynamics, the so called low-frequency shear layer flapping in the literature.

Separated boundary layer transition on a flat plate with a semi-circular leading edge under different Reynolds number and free-stream conditions, the so called ERCOFTAC T3L test cases, have been studied both experimentally and numerically by many researchers. The T3L test cases have been used to assess many turbulence models from the linear and non-linear eddy-viscosity models (Palikaras et al., 2002, 2003; Corsini and Rispoli, 2002; Cutrone et al., 2008), an intermittency transport model (Vicedo et al., 2004) to the second-moment closure (SMC) models (Hadzic and Hanjalic, 1999, Borello et al., 2005, Vlahostergios et al., 2007). The results show that good predictions regarding the reattachment point, the velocity and u-rms distributions inside the bubble could be obtained for the cases where FST is moderate or high. The general conclusion is that turbulence modelling can provide quite accurate results for transitional flows without any additional ad-hoc modifications. However, neither the experimental study (Coupland and Brierley, 1996; Palikaras et al., 2002, 2003) nor the above numerical studies investigated the transition mechanism and the shedding modes. Yang and Voke (2001) performed LES of a T3L test case (with very low FST) and presented detailed analysis of the transition mechanism. They demonstrated that the primary instability originated from the free shear layer in the bubble was due to the Kelvin–Helmholtz mechanism. A low frequency peak was also identified in the velocity spectra.

Several DNS studies of transition to turbulence within a laminar separation bubble have been carried out to investigate the transition mechanism (Alam and Sandham, 2000; Spalart and Strelets, 2000; Marxen et al., 2003, 2004). Three-dimensionality appeared very rapidly in the study of Spalart & Strelets with no clear regions of primary or secondary instability, whereas Alam & Sandham observed Λ-vortex-induced breakdown. Both studies concluded that the magnitude of the reverse flow was not sufficient to sustain absolute instability. Marxen et al. concluded that transition was driven by convective amplification of a two-dimensional TS wave and the dominant mechanism behind transition was an absolute secondary instability. Very recently, Jones et al. (2008) performed DNS of laminar separation bubbles on a NACA-0012 airfoil and they showed that the separation bubble was convectively unstable by classical linear stability analysis of the time-averaged flow fields. They also performed a series of three-dimensional simulations which illustrated a three-dimensional absolute instability of

* Corresponding author. Tel.: +44 (0)1509 227231.
E-mail address: z.yang@iboro.ac.uk (Z. Yang).

0142-727X/$ - see front matter © 2009 Elsevier Inc. All rights reserved.
doi:10.1016/j.ijheatfluidflow.2009.04.010

Notations

D	plate thickness	u_{rms}	root mean square value of streamwise velocity
f	frequency	V	normal velocity
FST	free-stream turbulence	v_{rms}	root mean square value of normal velocity
i	streamwise axis index	W	spanwise velocity
j	normal axis index	x	streamwise axis
k	spanwise axis index	x_R	mean separation bubble length
LES	large-eddy simulation	y	normal axis
NFST	no free-stream turbulence	z	spanwsie axis
SMC	second-moment closure	Δx^+	streamwise mesh size in wall units
TS	Tollmien–Schlichting	Δy^+	normal mesh size in wall units
U_0	free-stream velocity	Δz^+	spanwise mesh size in wall units
U	streamwise velocity	v_{eff}	effective viscosity

the two-dimensional vortex shedding that occurred naturally. However, the two shedding modes, especially the low-frequency shear layer flapping, were not shown in all those DNS studies.

Kiya and Sasaki (1983) studied turbulent separated–reattached flow under low free-stream turbulence over a blunt plate at a Reynolds number of 26,000 based on the free-stream velocity and the plate thickness. The measured power spectra of velocity and surface pressure fluctuation showed a peak band estimated about $fx_R/U_o = 0.6$–0.8 which they interpreted as the characteristic shedding frequency of the large-scale vortices from the free shear layer of the separation bubble. A long tail was also observed in the measured autocorrelation curve of velocity fluctuations at two positions shortly downstream of the separation up to the station $x/x_R = 0.5$. They suggested that the tail of the autocorrelation curve was associated with the low-frequency flapping motion of the shear layer near the separation line. They attributed the flapping to be a consequence of a large-scale unsteadiness in the bubble, which must be closely related to the shrinkage and enlargement of the separation bubble. They emphasised that this large-scale unsteadiness was different from the smaller-scale unsteadiness caused by the regular vortex shedding from the bubble, and the representative frequency of the former was much lower than that of the latter. Their measured surface pressure spectrum at $x/x_R = 0.2$ had a clear peak at $fx_R/U_o \approx 0.12$. The pressure spectra presented by Hillier and Cherry (1981a) had a peak at the same frequency in the region $0.026 < x/x_R < 0.25$ and they pointed out that this may be a result of flapping of the shear layer near the separation line. This low-frequency flapping ($fx_R/U_o \approx 0.12$) was further confirmed by Cherry et al. (1984).

Cherry et al. (1983), Castro and Haque (1987), Hudy et al. (2003) detected both the low and the characteristic frequency modes of unsteadiness for separated flow behind a normal flat plate with a long central splitter plate. However, Ruderich and Fernholz (1986) observed no dominant frequencies in their power spectra for the same flow configuration. In a backward-facing step flow, both the frequency modes were detected in velocity measurements of Eaton and Johnston (1981). They argued that the observed low-frequency motion on the backward-facing step flow was likely to be a consequence of an instantaneous imbalance between the entrainment rate from the recirculation zone and its resupply near the reattachment. Lee and Sung (2001) also detected the two modes in their measured spectra of surface pressure close to separation in a backward-facing step flow.

A separated–reattached flow over a blunt flat plate was studied by Cherry et al. (1984) at a Reynolds number of 32,000 based on the free-stream velocity and the plate thickness. However, the difference was that the flow was laminar before separation but transition occurred extremely close to separation. Near separation, the measured power spectra for surface-pressure fluctuations were found to be dominated by low-frequency fluctuations. The low frequency value was estimated to be about $fx_R/U_o \approx 0.12$ from the pressure spectrum at $x/D = 0.125$ (D is the flat plate thickness). They were suspicious that transition might be the cause of this. However, because transition at the test Reynolds number occurred extremely close to separation so that transition effect was ruled out. Due to the fact that this phenomenon appeared in a very similar case by Kiya and Sasaki (1983), in backward-facing step separations of both Eaton and Johnston (1981) and Lee and Sung (2001), and in the study by Cherry et al. (1983) where it was turbulent flow at separation in all those cases, Cherry et al. (1984) drew the conclusion that "the low-wave number motion appears to be an integral feature of fully turbulent separation". This conclusion has been supported by the study of Abdalla and Yang (2005) for the NFST case of a separated–reattached flow over a blunt flat plate where the flow at separation is laminar.

It has been established that FST has a great impact on a separated–reattached flow. Hillier and Cherry (1981b) showed that increasing FST level would produce considerable contraction of the bubble length which was, however, insensitive to turbulent length scale. Nakamura and Ozono (1987) reached similar conclusion after exploring the effect of turbulence length scales over a wider range. Kalter and Fernholz (2001) studied the effect of FST on a boundary layer with an adverse pressure gradient and a closed reverse-flow region. They found that by adding FST the mean reverse-flow region was shortened or completely eliminated. Yang and Abdalla (2005) investigated the effects of FST on large-scale coherent structures of separated boundary transition. They have found that some clearly identified coherent structures in the NFST case can hardly be identified under 2% free-stream turbulence and transition starts earlier for the FST case. However, all the above mentioned studies did not address the effect of FST on the low-frequency flapping of the shear layer. Only Castro and Haque (1988) mentioned in their study of a separated–reattached flow behind a normal flat plate with a long central splitter plate that FST led to an increased 'flapping motion' of the shear layer just after separation. In this paper we present and discuss results of a transitional separated–reattached flow under 2% FST, focusing on if the low-frequency flapping of the shear layer occurs in this case and what the mechanism is if it does occur.

2. Governing equations and the numerical methods

The implicitly filtered equations (due to the use of finite volume method there is no need to introduce an explicit filter) expressing conservation of mass and momentum in a Newtonian incompressible flow can be written in conservative form as

$$\partial_i \overline{u_i} = 0 \tag{1}$$

$$\partial_t(\bar{u}_i) + \partial_j(\bar{u}_i\bar{u}_j) = -\partial_i\bar{p} + 2\partial_j(v_{eff}\overline{s_{ij}}) \tag{2}$$

where $\bar{p}$ is the filtered pressure divided by density and v_{eff} is the effective viscosity (molecular viscosity + subgrid scale viscosity) and $\overline{s_{ij}}$ is

$$\overline{s_{ij}} = \frac{1}{2}(\partial_i\overline{u_j} + \partial_j\overline{u_i}) \tag{3}$$

The Poisson equation for pressure can be derived by taking the divergence of Eq. (2)

$$\partial_i\partial_t(\overline{u_i}) + \partial_i\partial_j(\bar{u}_i\bar{u}_j) = -\partial_i\partial_i\bar{p} + 2\partial_i\partial_j(v_{eff}\overline{S_{ij}}) \tag{4}$$

And using Eq. (1) one finally obtains

$$\partial_i\partial_i\bar{p} = \Delta^2\bar{p} = \partial_i H_i \tag{5}$$

where

$$H_i = \partial_j(-\bar{u}_i\bar{u}_j + 2v_{eff}\overline{S_{ij}}) \tag{6}$$

Generally speaking, it is computationally very expensive to solve Eq. (5) for high Reynolds turbulent flows and one way to speed up the solution is to Fourier transform the equation in z direction to obtain a set of decoupled 2D equations, which in Cartesian form is given by

$$\frac{\partial^2\tilde{p}}{\partial^2 x} + \frac{\partial^2\tilde{p}}{\partial^2 y} - k_z^2\tilde{p} = \tilde{R} \tag{7}$$

Provided flow is homogeneous in z direction so that a periodic boundary condition can be applied. k_z is the discrete Fourier wave number given as

$$k_z = \frac{2\sin(k_z/2)}{\Delta z} \tag{8}$$

The two-dimensional Eq. (7), one for each value of k_z, can be solved very quickly even when the geometry is complex as long as flow is homogeneous in z direction.

The numerical methods used in the present studies are direct descendants of well-known finite-volume techniques successfully used for many LES studies. A standard dynamic subgrid-scale model is used to approximate the subgrid-scale stresses. The explicit second order Adams–Bashforth scheme is used for the momentum advancement except for the pressure term. The Poisson equation for pressure is solved using an efficient hybrid Fourier multi-grid method. The spatial discretization is second-order central differencing which is widely used in LES owing to its non-dissipative and conservative properties. More details of the mathematical formulation and numerical methods have been reported elsewhere by Yang and Voke (2000).

3. Details of numerical computation

The computational domain and mesh used in the current study are shown in Fig. 1. The computational domain size is $25D \times 16D \times 4D$ along the x-, y- and z-axis respectively where D = 10.0 mm is the plate thickness. The Reynolds number based on the free-stream velocity and plate thickness is 6500. The x-coordinate origin is located $0.5D$ from the leading edge of the plate and hence the inflow boundary is at $x = -4.5D$. The outflow boundary is at $x = 20.5D$. The lateral boundaries are at $y = -8D$ and $y = 8D$, corresponding to a blockage ratio of 1/16.

The mesh refinement study had been done for the NFST case with two simulations performed by Abdalla and Yang (2005). Results in terms of flow structures, spectra and even the mean first order quantities showed little difference and the mean second order quantities showed a maximum difference around 4%. Since the FST case has the same geometry and the same Reynolds number as in the NFST case so that the finer mesh used in the NFST case should also be adequate for the FST case. The grid is consisting of $256 * 212 * 64$ cells along the streamwise, wall-normal and spanwise directions respectively. Non-uniform grid distributions were used in the x- and y-directions and a uniform grid distribution was used in the spanwise direction. In terms of wall units based on the friction velocity downstream of reattachment at $x/x_R = 2.5$ the streamwise mesh sizes vary from $\Delta x^+ = 9.7$ to $\Delta x^+ = 48.5$, $\Delta z^+ = 20.2$ and at the wall $\Delta y^+ = 2.1$, justifying the use of no-slip wall boundary condition. Yang and Voke (2001) did a study on the effects of the location of the spanwise periodic planes (two spanwise dimensions were used, 2D and 4D) in a very similar type of flow (flow over a flat plate with a semi-circular leading edge) and did not find any appreciable change in the behaviour of the flow (less than 5% difference in terms of averaged statistics for both mean and turbulence stresses). Hence the spanwise dimension, 4D, is regarded as sufficient in the present study. The time step used in this simulation was $0.001885D/U_0$. The simulation ran for 91,400 time steps to allow the transition and turbulent boundary layer to become established, i.e., the flow reached a statistically stationary state, and the averaged results were gathered over further

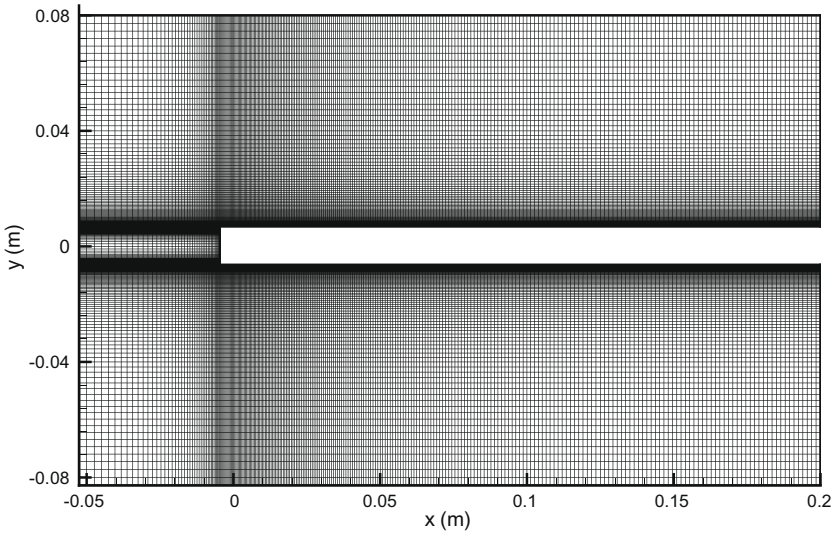

Fig. 1. Computational domain and mesh.

159,990 steps, with a sample taken every 10 time steps (15,999 samples) and averaged over the spanwise direction too, corresponding to around 11 flow-through or residence times. The code is highly efficient as the Poisson equation for pressure is solved using a hybrid Fourier multi-grid which results in a speedup of at least five times compared with a fully 3D Poisson solver.

On the lateral boundaries a free-slip but impermeable boundary condition was applied. Periodic boundary conditions were used in the spanwise direction. No-slip boundary conditions were used at all walls. A convective boundary condition was applied at the outflow boundary. At inlet realistic turbulence needed to be specified to mimic the 2% FST at the leading of the plate which was very difficult to generate numerically. Up to date there are no universal efficient methods to generate realistic turbulent inflow data. Several methods have been tried in the present study but they are not very satisfactory (some of those techniques require not only first order and second order turbulent quantities but also turbulent length scales etc. which are not available). As a result, the so called "precursor technique" was employed, i.e., an additional channel flow simulation was performed to provide realistic turbulent inlet conditions. Fig. 2 shows the computational domain and mesh of the channel flow simulation. The domain size in the y-direction was slightly larger than that of the main simulation and exactly the same mesh used in the main simulation was employed with additional 80 cells added in the near wall region (40 on each side) to resolve the boundary layer (the first mesh point is located at about $y^+ = 1.2$), leading to a total of 292 cells along the y-direction, 64 cells along the streamwise and spanwise directions. Periodic boundary conditions were used along the streamwise and spanwise directions. The bulk velocity in the precursor simulation was the same as the free-stream velocity in the main simulation (i.e. 9.425 m/s) and the Reynolds number based on the bulk velocity and half channel height is 65,000. Turbulence was extracted (fluctuation part of the axial velocity and instantaneous velocity components in other two directions) from the channel flow and fed to the main simulation after the channel flow reached a fully developed state. In order to avoid the situation where the precursor simulation may feed its own "recycling" frequency into the main simulation 400,000 slices were stored to make sure that those slices should be used only once.

In the channel flow turbulence intensity reaches a peak value close to the wall and reduces towards the centre with the minimum value at the centre. The average turbulence intensity over the bulk region of the channel in the current case from $y = -0.08$ m to $y = 0.08$ m was about 5.9% which was fed to the main simulation at inflow boundary located at $x = -4.5D$ (0.045 m). It decayed fairly rapidly downstream the inflow plane and the average turbulence intensity reduced to about 2% just upstream of the plate (the plate leading edge is at $x = 0$) and the turbulence intensity profile was fairly flat and not changing much at all in the y direction. The ratio of turbulence normal stresses was about $u':v':w' = 1.0:0.83:0.94$ at the leading edge of the plate. This is not exactly the same as the grid turbulence but not far from it.

4. Results and discussion

4.1. Mean flow variables

In a separated–reattached flow the mean separation bubble length is an important parameter and it has been found experimentally, as mentioned before, that the mean separation bubble length can be substantially reduced by the free-stream turbulence (Hillier and Cherry, 1981b; Nakamura and Ozono, 1987; Castro and Haque, 1988; Kalter and Fernholz, 2001). The predicted mean bubble length in the current study for the FST case is 5.6D while for the NFST case it is 6.5D, leading to a 14% reduction due to 2% FST, confirming that the current predictions are consistent with the experimental results.

Fig. 3 presents the comparison between the predicted mean streamwise velocity profiles and the experimental data by Kiya

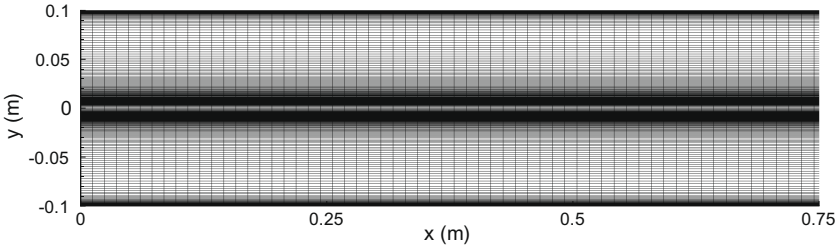

Fig. 2. Computational domain and mesh of the precursor simulation.

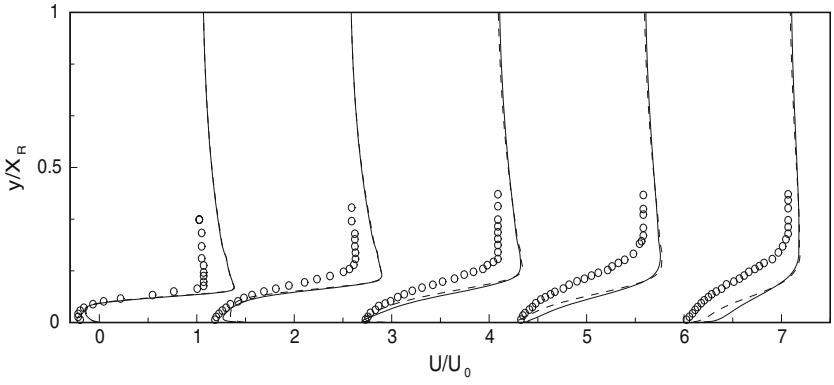

Fig. 3. Mean axial velocity profiles at five streamwise locations measured from the leading edge. Left to right, $x/x_R = 0.2, 0.4, 0.6, 0.8, 1.0$. Solid line, LES (FST case); dashed line, LES (NFST case); symbols, experimental data.

and Sasaki (1983) at five streamwise locations for both the FST & NFST cases, normalised by the free-stream velocity. It is worth pointing out that the experiment was carried out with very low free-stream turbulence level but at a higher Reynolds number (26,000) and the measured reattachment length was 5.05D. The mean bubble length is Reynolds number dependent as Cherry et al. (1984) reported a measured value of around 4.9D for a Reynolds number of about 32,000 and Djilali and Gartshore (1991) measured a value of about 4.7D at a Reynolds number of 50,000. To facilitate comparisons the profiles are plotted as function of y/x_R at corresponding values of x/x_R, i.e., comparisons are made at the same non-dimensionalised location (x/x_R) but not at the same geometric location (x). A reasonably good agreement has been obtained between the experimental data and the LES predictions for both the FST and NFST cases, as shown in Fig. 3. Both the predicted peak and the free stream values of the velocity are slightly bigger than those measured by Kiya and Sasaki (1983). The discrepancy could be due to the differences in blockage ratio (1/20 in the experiment and 1/16 in the current study), due to the Reynolds number differences (26,000 in the experiment and 6500 in the current study) and also due to the fact that it was turbulent separation at the leading edge in the experiment while it is laminar separation in the current study (even for the FST case as shown later). The predictions for both the FST and the NFST cases are very similar, especially at the first two stations the results for both cases are almost identical. This indicates that 2% FST does not have a noticeable impact on the mean velocity at all, also indicating that flow is still laminar at separation for the FST case.

Fig. 4 shows the comparison between the predicted profiles of the rms of streamwise velocity and the experimental data by Kiya and Sasaki (1983), normalised by U_0 at the same five streamwise locations. The effects of FST can be clearly identified as the predicted results in the FST case show not only higher values far away from the wall in the free stream, which can only be due to free-stream turbulence at inlet, but also higher peak values near the wall compared with the results in the NFST case. At the first two stations the predictions for the FST case agree better with the experimental data than the NFST results, implying that transition may occur slightly earlier due to 2% FST. However, at the other three stations the FST results show a slightly higher peak value compared with the experimental data whereas a slightly better agreement is obtained between the NFST results and the experimental data in the near wall region. The peak value locations are better captured in the FST case. At the first location the predictions for both cases are very similar and the peak values are quite close to each other, confirming that the flow is still laminar at separation for the FST case as mentioned above.

The comparison between the predicted u_{rms}, v_{rms}, $-uv$ and the experimental data by Kiya and Sasaki (1983) at the mean reattachment location is presented in Fig. 5. Due to FST, as expected, the predicted u_{rms} and v_{rms} in the FST case are slightly higher compared with the results in the NFST case. However, the predicted shear stress is much higher in the FST case. A reasonably good agreement bas been obtained between the LES results in both cases and the experimental data for u_{rms} and v_{rms}. However, there is larger discrepancy between the predicted results and the experimental data for shear stress as it is over-predicted in the FST case and under-predicted in the NFST case. Furthermore, the predicted peak value locations are all closer to the wall compared with the experimental peak value locations, the impact of FST can still be identified at this location where transition has more or less finished.

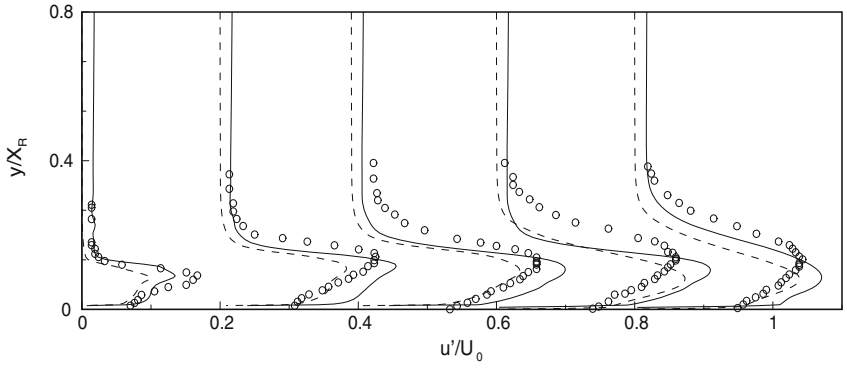

Fig. 4. Axial velocity fluctuations rms profiles at five streamwise locations measured from the leading edge. Left to right, x/x_R = 0.2, 0.4, 0.6, 0.8, 1.0. Solid line, LES (FST case); dashed line, LES (NFST case); symbols, experimental data.

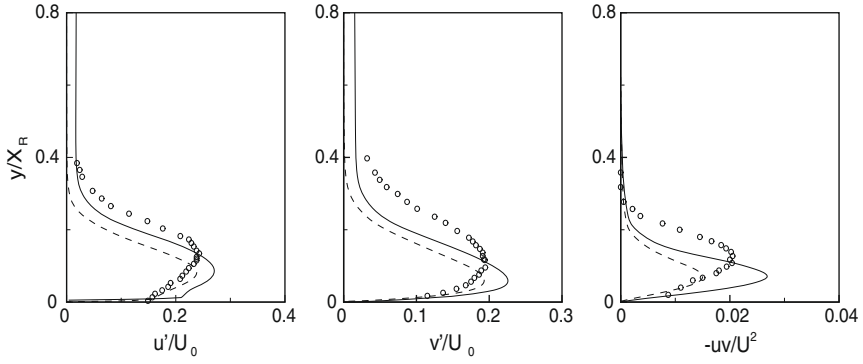

Fig. 5. Velocity fluctuations rms and Reynolds shear stresses at the mean reattachment location. Solid line, LES (FST case); dashed line, LES (NFST case); symbols, experimental data.

4.2. Transition process

The effects of FST on the overall transition process can be seen from Fig. 6 which shows a snap shot of the instantaneous spanwise vorticity in the (*x*, y) plane for the NFST case (a) and FST case (b) at the mid-span location (it looks very similar at other spanwise locations). Flow separates at the leading edge and a stable free shear layer develops initially for both cases. However, at certain region downstream the free shear layer is inviscidly unstable via the Kelvin–Helmholtz mechanism and any small disturbances present grow downstream with an amplification rate larger than that in the case of viscous instabilities. Further downstream, the initial formed 2D spanwise vortices are distorted severely and roll up, leading to streamwise vorticity formation associated with significant 3D motions, eventually breaking down into relatively smaller turbulent structures at about the reattachment point and developing into a turbulent boundary layer rapidly afterwards. For the FST case the transition and the breakdown of the separated boundary layer occurs earlier than in the NFST case and some of the clearly identified 3D vortical structures such as Lambda-shaped vortices in the NFST case can hardly be identified in the FST case (Yang and Abdalla, 2005).

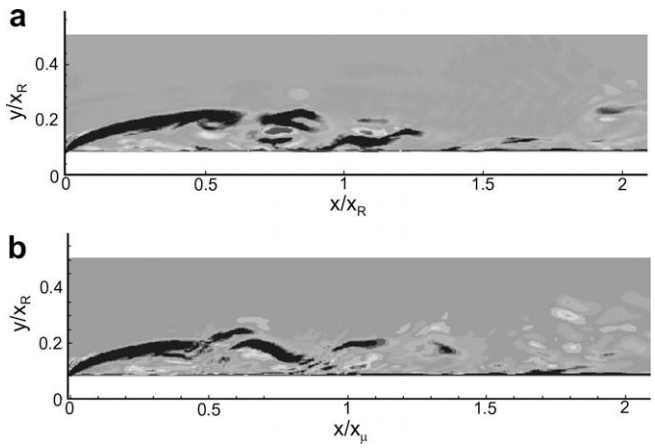

Fig. 6. Instantaneous spanwise vorticity: (a) NFST case; (b) FST case.

4.3. Pressure spectra

In order to elucidate if the low-frequency flapping may occur in the current study (under 2% FST) LES data stored at seven streamwise locations were processed to get the velocity and pressure spectra. The streamwise locations are: $x/x_R = -0.05$, 0.05, 0.25, 0.5, 0.75, 1.0, 1.25, and also at two spanwise locations: $z/x_R = 0.2$, 0.4. At each streamwise and spanwise location, time traces of velocities were stored at four wall-normal locations: $y/x_R = 0.01$, 0.05, 0.13 and 0.2. Those four wall-normal positions were chosen to include the very near wall region, around centre of the mean separation bubble height, edge of the mean free shear layer at $x/x_R = 0.5$, and in the free stream, with a total of 56 points. The results presented below correspond to 19,870 samples at each point (taken every 10 time-steps) equivalent to 0.3974 seconds, enough samples to provide reliable results over the relevant shedding frequency range (the maximum frequency that can be resolved is 25 kHz and the lowest is about 5 Hz) as the typical low-frequency flapping occurs at about $fx_R/U_o \approx 0.12$ (Hillier and Cherry, 1981a; Kiya and Sasaki, 1983; Cherry et al., 1984). Based on the current data ($x_R = 0$ .056 m and $U_o = 9.425$ m/s), this is equivalent to 20.2 Hz or the low-frequency flapping would happen every 0.0495 s which means that the samples collected over a length of 0.3974 s are able to cover more than eight low-frequency flapping cycles and should have been able to capture this low-frequency flapping if it exists in the current study.

Results shown below are at $z/x_R = 0.4$ (about the central location in the spanwise direction) since results at $z/x_R = 0.2$ are very

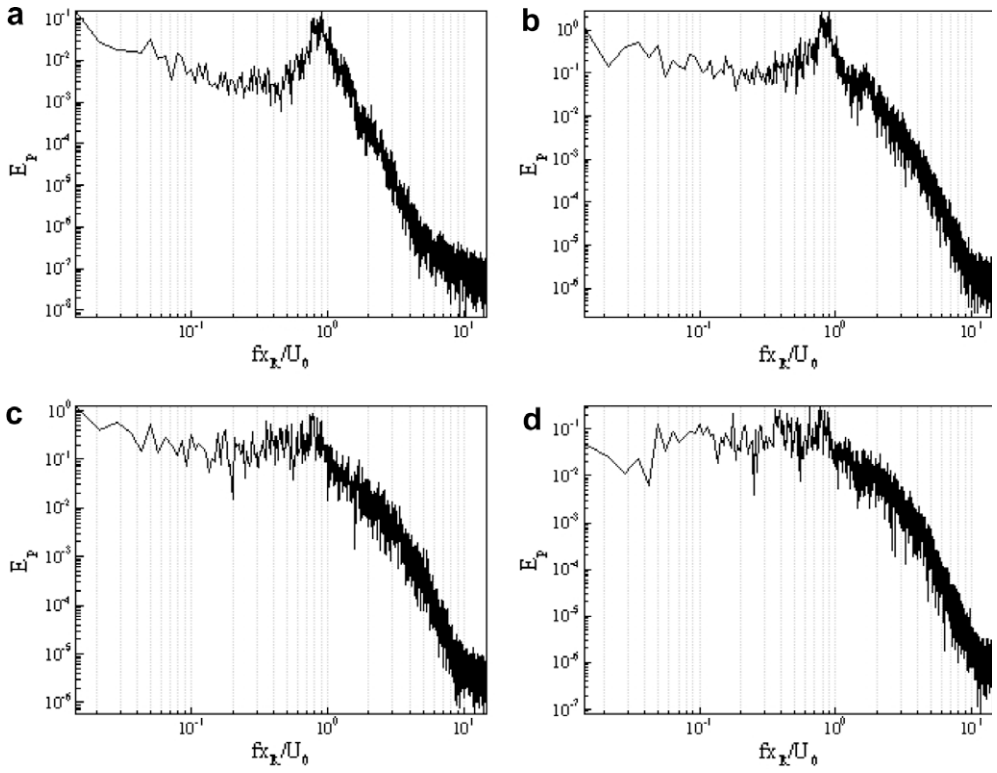

Fig. 7. The pressure spectra at $x/x_R = 0.05$ and at $y/x_R = 0.01$ (a), $y/x_R = 0.05$ (b), $y/x_R = 0.13$ (c), $y/x_R = 0.2$ (d).

similar. It has been found that the pressure spectra show a peak clearly at almost all locations while this peak can only be vaguely identified at certain locations in the velocity spectra so that only the pressure spectra are presented below.

Fig. 7 shows the pressure spectra at $x/x_R = 0.05$ and at four wall-normal locations: $y/x_R = 0.01, 0.05, 0.13$ and 0.2 (from the very near wall region to the free stream area). It can be seen clearly from Fig. 7a ($y/x_R = 0.01$) and Fig. 7b ($y/x_R = 0.05$) that there is small band of peak frequencies at about $0.8–0.9U_0/x_R$. This is close to the characteristic shedding frequencies, $0.6–0.8U_0/x_R$ measured by Kiya and Sasaki (1983), and $0.78U_0/x_R$ measured by Cherry et al. (1984). This peak frequency band corresponding to the characteristic frequencies is

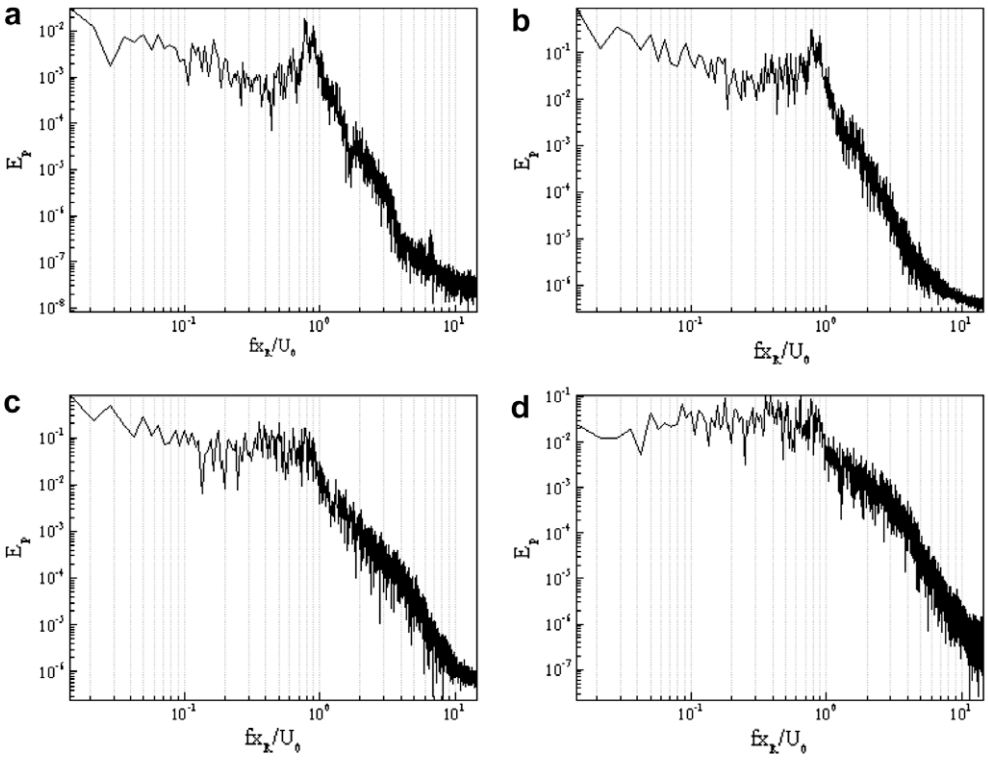

Fig. 8. The pressure spectra at $x/x_R = 0.25$ and at $y/x_R = 0.01$ (a), $y/x_R = 0.05$ (b), $y/x_R = 0.13$ (c), $y/x_R = 0.2$ (d).

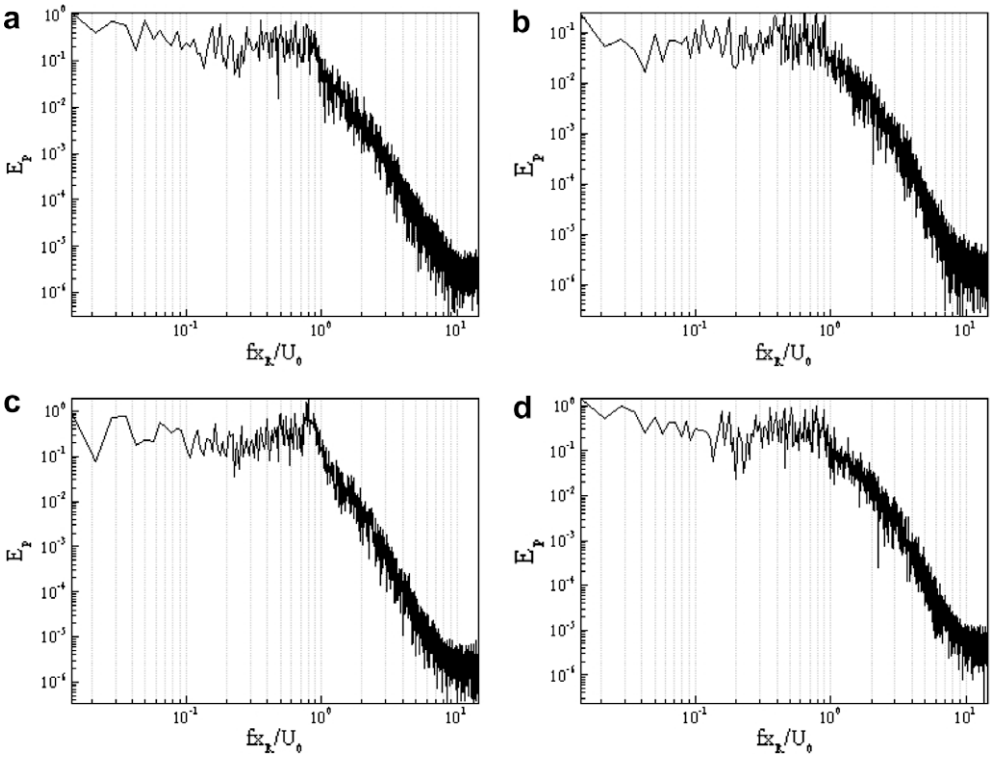

Fig. 9. The pressure spectra at $x/x_R = 0.5$ and at $y/x_R = 0.01$ (a), $y/x_R = 0.05$ (b), $y/x_R = 0.13$ (c), $y/x_R = 0.2$ (d).

not so apparent in Fig. 7c ($y/x_R = 0.13$) and can be hardly identified in Fig. 7d ($y/x_R = 0.2$). However, there is no sign of any apparent low frequency peak band at around $0.12U_0/x_R$ as shown in the measured pressure spectra by Kiya and Sasaki (1983), Hillier and Cherry (1981a) and Cherry et al. (1984).

Fig. 8 presents the pressure spectra at $x/x_R = 0.25$ and at the same four wall-normal locations as in Fig. 7. The spectra show clearly a small band of peak frequencies at two wall-normal locations, $y/x_R = 0.01$ and $y/x_R = 0.05$, and the frequency rang is the same as that shown in Figs. 7a and b ($0.8–0.9U_0/x_R$), close to the

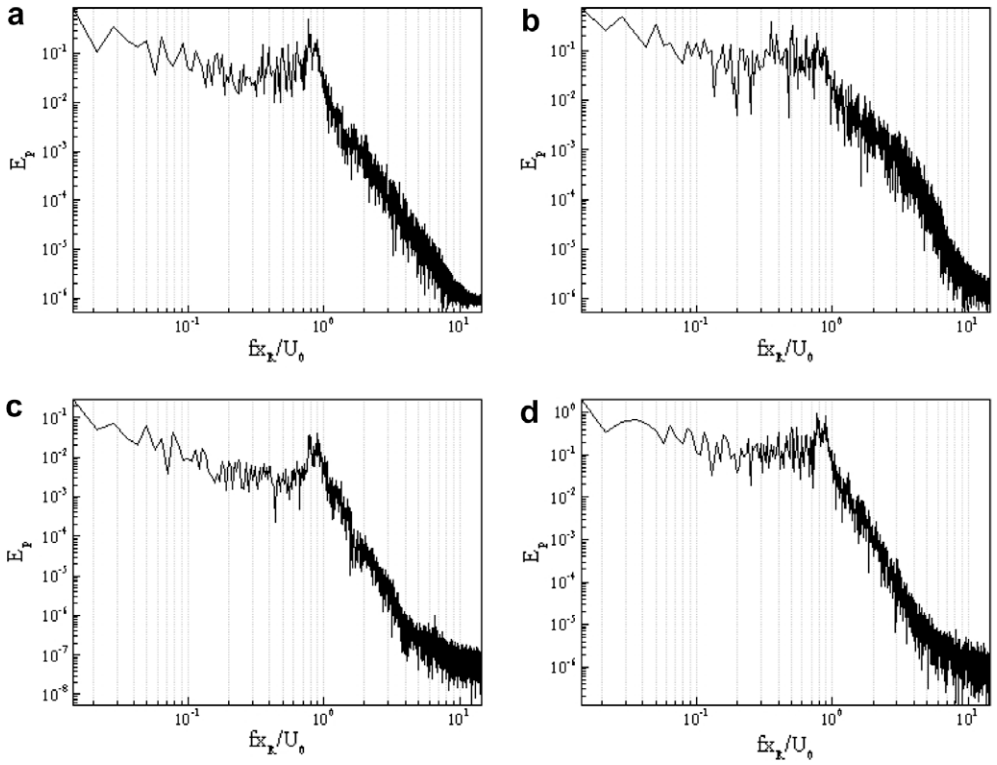

Fig. 10. The pressure spectra at $x/x_R = 0.75$ and at $y/x_R = 0.01$ (a), $y/x_R = 0.05$ (b), $y/x_R = 0.13$ (c), $y/x_R = 0.2$ (d).

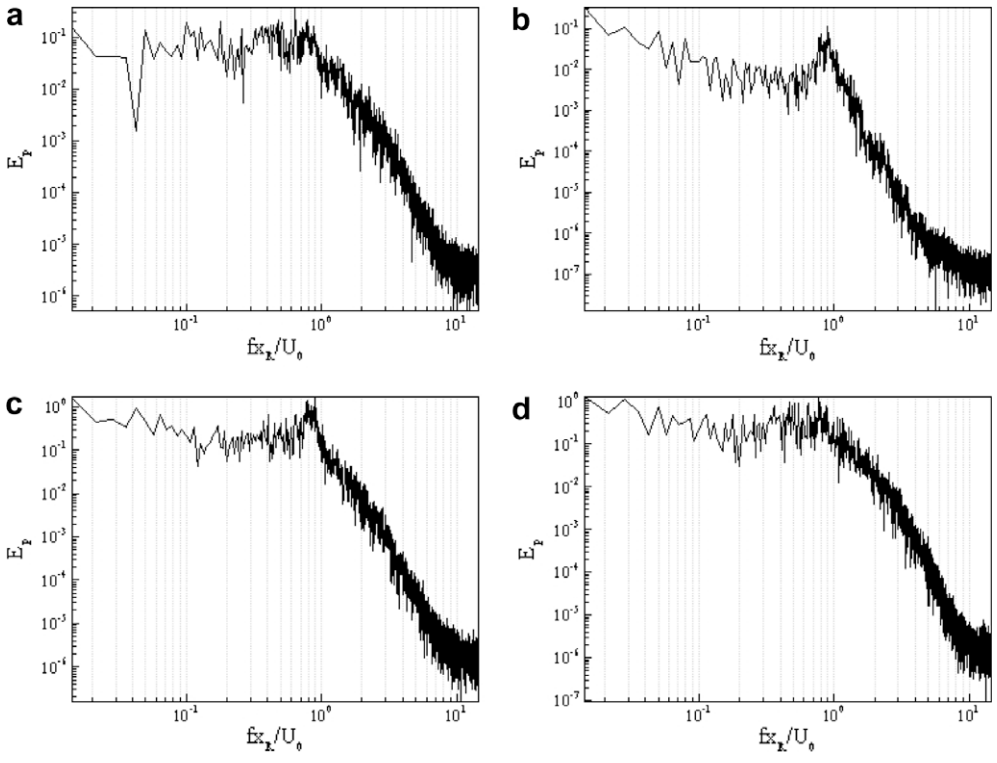

Fig. 11. The pressure spectra at $x/x_R = 1.0$ and at $y/x_R = 0.01$ (a), $y/x_R = 0.05$ (b), $y/x_R = 0.13$ (c), $y/x_R = 0.2$ (d).

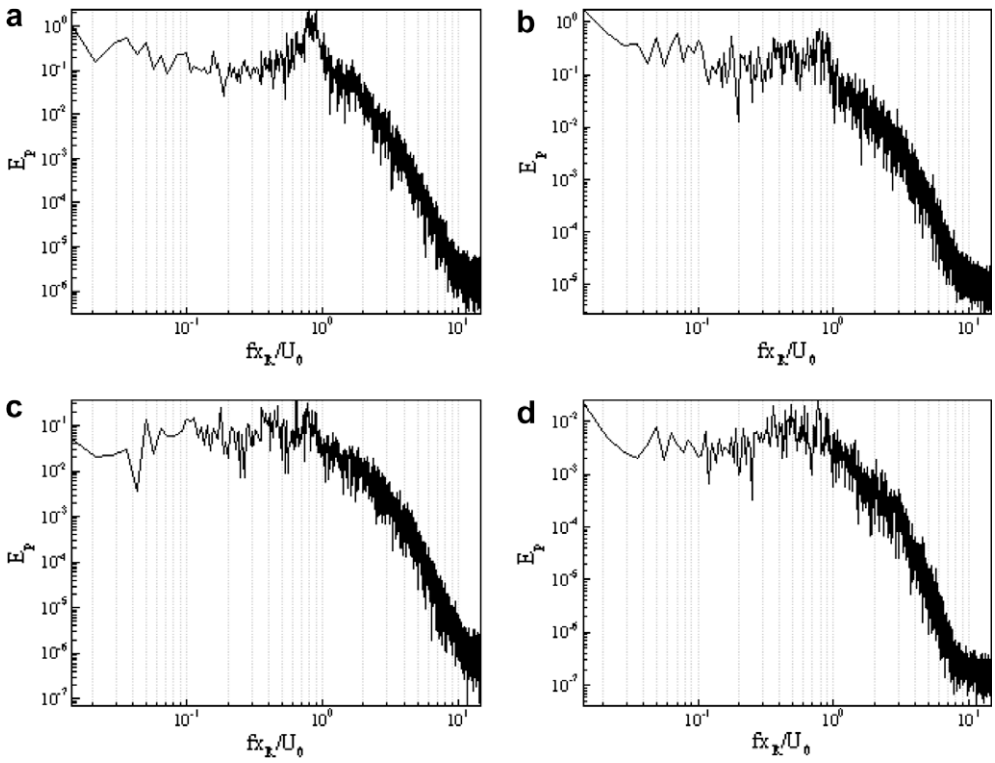

Fig. 12. The pressure spectra at $x/x_R = 1.25$ and at $y/x_R = 0.01$ (a), $y/x_R = 0.05$ (b), $y/x_R = 0.13$ (c), $y/x_R = 0.2$ (d).

measured characteristic shedding frequencies. Further away from the wall at $y/x_R = 0.13$ and $y/x_R = 0.2$ this peak frequency band is not clearly detected as shown in Figs. 8c and d. The low frequency peak observed in the measured pressure spectra does not appear.

The pressure spectra at $x/x_R = 0.5$ and at the same four wall-normal locations are shown in Fig. 9. The same frequency peak band can only be clearly identified at $y/x_R = 0.13$ while it can hardly be seen at other three wall-normal locations. Again, the pressure spectra at this streamwise location do not show any low frequency peak. Going further downstream at $x/x_R = 0.75$ this characteristic shedding frequency band ($0.8–0.9U_0/x_R$) is clearly observable at three wall-normal locations, $y/x_R = 0.01$, 0.13 and 0.2 as shown in Figs. 10a,c and d. There is no low frequency peak at around $0.12U_0/x_R$ at this location either.

Fig. 11 shows the pressure spectra at $x/x_R = 1.0$ and at the same four wall-normal locations and the same peak frequency band ($0.8–0.9U_0/x_R$) corresponding to the characteristic frequencies discussed above is clearly visible at $y/x_R = 0.05$ (Fig. 11b) and $y/x_R = 0.13$ (Fig. 11c). Further downstream the mean attachment point at $x/x_R = 1.25$ this peak frequency band only appears clearly at the very wall region, $y/x_R = 0.13$, as shown in Fig. 12a. Similar to other streamwise locations the low frequency peak ($0.12U_0/x_R$) shown clearly in the measured pressure spectra by Kiya and Sasaki (1983), Hillier and Cherry (1981a) and Cherry et al. (1984) cannot be identified.

5. Conclusion

A transitional separated–attached flow over a blunt flat plate under 2% FST has been investigated numerically using the Large-eddy simulation approach. A dynamic subgrid scale model is employed to approximate the unresolved subgrid-scale motion. Several methods were tried to artificially generate turbulent inflow data but were not satisfactory and the so called precursor method was used to provide realistic turbulence with 2% turbulence intensity at around the plate leading edge. The LES results compare reasonably well with the available experimental data and the 2% FST resulted in a 14% reduction in the mean reattachment length compared with the NFST case. This is consistent with most of the experimental work performed on the blunt plate geometry.

From the thorough spectra analysis from the current study the low-frequency flapping is not present in the current study under 2% FST. This low-frequency mode has been detected in several experimental studies of turbulent separation at the blunt leading edge. Although the current study is under 2% FST the flow at the leading edge is still laminar (laminar separation) so that this low-frequency mode in separated–reattached flows may only appear in the case of turbulent separation as suggested by Cherry et al. (1984). A peak frequency band at about $0.8–0.9U_0/x_R$ is clearly visible in the pressure spectra and this peak frequency band is close to the characteristic shedding frequencies, $0.6–0.8U_0/x_R$, measured by Kiya and Sasaki (1983), and $0.78U_0/x_R$ measured by Cherry et al. (1984).

The addition of 2% FST has produced more chaotic motion in the free shear layer, causing earlier transition. The results indicate that if the level of FST is raised further, a much more rapid transition may occur with a different transition mechanism, similar to the so called bypass transition in attached boundary layer flow. However, under the current 2% FST level the shedding still occurs with a characteristic shedding frequency equivalent to the value in the NFST case. This indicates that the primary instability mechanism of the NFST case (Kelvin–Helmholtz instability) is working here too.

References

Abdalla, I.E., Yang, Z., 2005. Numerical study of a separated–reattached flow on a blunt plate. AIAA J. 43, 2465–2474.

Alam, M., Sandham, N.D., 2000. Direct numerical simulation of short laminar separation bubbles with turbulent reattachment. J. Fluid Mech. 410, 1–28.

Borello, D., Hanjalic, K., Rispoli, F., 2005. Prediction of cascade flows with innovative second-moment closures. J. Fluid Eng. 127, 1059–1070.

Castro, I.P., Haque, A., 1987. The structure of a turbulent shear layer bounding a separation region. J. Fluid Mech. 179, 439–468.

Castro, I.P., Haque, A., 1988. The structure of a shear layer bounding a separation region. Part 2. Effects of free-stream turbulence. J. Fluid Mech. 192, 577–595.
Cherry, N.J., Hillier, R., Latour, M.E.M.P., 1983. The unsteady structure of two-dimensional separated and reattaching flows. J. Wind Eng. Ind. Aerodynam. 11, 95–105.
Cherry, N.J., Hillier, R., Latour, M.E.M.P., 1984. Unsteady measurements in a separating and reattaching flow. J. Fluid Mech. 144, 13–46.
Corsini, A., Rispoli, F., 2002. Anisotropic turbulence modelling of near wall effects pertinent to turbomachinery. ASME Paper FEDSM02, Montreal.
Coupland, J., Brierley, D., 1996. Transition in turbomachinery flows. Final Report, BRITE/EURAM Project AERO-CT92-0050.
Cutrone, L., Palma, P.De., Pascazio, G., Napolitano, M., 2008. Predicting transition in two- and three-dimensional separated flows. Int. J. Heat Fluid Flow 29, 504–526.
Djilali, N., Gartshore, I.S., 1991. Turbulent flow around a bluff rectangular plate Part I: experimental investigation. ASME J. Fluid Eng. 113, 51–59.
Eaton, J.K., Johnston, J.P., 1981. A review on subsonic turbulent flow reattachment. AIAA J. 19, 1093–1100.
Hadzic, I., Hanjalic, K., 1999. Separation-induced transition to turbulence: second-moment closure modelling. Flow Turbul. Combust. 63, 153–173.
Hillier, R., Cherry, N.J., 1981a. Pressure fluctuations under a turbulent shear layer. In: Proceedings of the third Turbulent Shear Flow Symposium, Davis, California, September, pp. 23–29.
Hillier, R., Cherry, N.J., 1981b. The effects of free-stream turbulence on separation bubbles. J. Wind Eng. Ind. Aerodynam. 8, 49–58.
Hudy, L.M., Naguib, A.M., Humphreys, W.M., 2003. Wall-pressure-array measurements beneath a separating/reattaching flow region. Phys. Fluid. 15, 706–717.
Jones, L.E., Sandberg, R.D., Sandham, N.D., 2008. Direct numerical simulation of forced and unforced separation bubble on an airfoil at incidence. J. Fluid Mech. 602, 175–207.
Kalter, M., Fernholz, H.H., 2001. The reduction and elimination of a closed separation region by free-stream turbulence. J. Fluid Mech. 446, 271–308.
Kiya, M., Sasaki, K., 1983. Structure of a turbulent separation bubble. J. Fluid Mech. 137, 83–113.
Lee, I., Sung, H.J., 2001. Characteristics of wall pressure fluctuations in separated and reattaching flow over a backward-facing step. Exp. Fluid. 30, 262–272.
Marxen, O., Lang, M., Rist, U., Wagner, S., 2003. A combined experimental/numerical study of unsteady phenomena in a laminar separation bubble. Flow Turbul. Combust. 71, 133–146.
Marxen, O., Rist, U., Wagner, S., 2004. Effect of spanwise-modulated disturbances on transition in a separated boundary layer. AIAA J. 42, 937–944.
Nakamura, Y., Ozono, S., 1987. The effects of turbulence on a separated and reattaching flow. J. Fluid Mech. 178, 477–490.
Palikaras, A., Yakinthos, K., Goulas, A., 2002. Transition on a flat plate with a semi-circular leading edge under uniform and positive free-stream flow. Int. J. Heat Fluid Flow 23, 455–470.
Palikaras, A., Yakinthos, K., Goulas, A., 2003. The effect of negative shear on the transitional separated flow around a semi-circular leading edge under uniform and positive free-stream flow. Int. J. Heat Fluid Flow 24, 241–430.
Ruderich, R., Fernholz, H.H., 1986. An experimental investigation of a turbulent shear flow with separation, reverse flow and reattachment. J. Fluid Mech. 163, 283–322.
Spalart, P.R., Strelets, M.K.H., 2000. Mechanism of transition and heat transfer in a separation bubble. J. Fluid Mech. 403, 329–349.
Vicedo, J., Vilmin, S., Dawes, W.N., Savill, A.M., 2004. Intermittency transport modelling of separated flow transition. J. Turbomach. 126, 424–431.
Vlahostergios, Z., Yakinthos, K., Goulas, A., 2007. Experience gained using second-moment closure modelling for transitional flows due to boundary layer separation. Flow Turbul. Combust. 79, 361–387.
Yang, Z., Abdalla, I.E., 2005. Effects of free-stream turbulence on large-scale coherent structures of separated boundary layer transition. Int. J. Numer. Meth. Fluid. 49, 331–348.
Yang, Z., Voke, P.R., 2000. Large-eddy simulation of separated leading-edge flow in general co-ordinates. Int. J. Numer. Meth. Eng. 49, 681–696.
Yang, Z., Voke, P.R., 2001. Large-eddy simulation of boundary layer separation and transition at a change of surface curvature. J. Fluid Mech. 439, 305–333.